Biomass Conversion and Biorefinery (2025) 15:25093–25106
https://doi.org/10.1007/s13399-025-06797-x

ORIGINAL ARTICLE

Effect of sorption parameters on the removal of malachite green with modified *Juniperus Excelsa* cone biochar

Uğur Özkan[1] · Okan Bayram[2] · Halil Turgut Şahin[1]

Received: 14 January 2025 / Revised: 7 March 2025 / Accepted: 18 March 2025 / Published online: 2 April 2025
© The Author(s) 2025

Abstract

The use of biochar, which is a carbon-rich material obtained by pyrolysis of various organic raw materials for dye pollution in wastewater, is promising for the removal of dyes from wastewater. Modified biochars whose structures are changed are currently being investigated with many studies. In this study, *Juniperus Excelsa* (JE) cone, which is an economical and accessible tree species, was converted into biochar (JEB) and modified with iron (mJEB) and given magnetic properties. mJEB was characterized and its structure was investigated by Brunauer–Emmett–Teller (BET), X-Ray diffraction method (XRD), Fourier transform infrared spectroscopy (FT-IR), scanning electron microscopy (SEM), and point of zero charge (pH_{PZC}). Afterwards, the removal of malachite green (MG) dye by batch adsorption method was investigated in adsorption parameters such as pH, temperature, time, dosage, initial MG concentration. The results showed that MG adsorption with mJEB proceeded via pseudo-second-order (PSO), was an endothermic process and complied with the Langmuir isotherm model. The maximum adsorption capacity (q_{max}) in MG removal with mJEB was calculated as 38.023 mg/g. Our study will be an important step in dye removal studies with mJEB.

Keywords *Juniperus Excelsa* · Adsorption · Malachite green · Biochar

1 Introduction

Water, a vital and indispensable resource for living things, is important in various sectors and industries [1–3]. However, accelerating socio-economic development and increasing human activities have made water management face significant challenges. Various by-products and wastes generated as a result of these activities often enter natural water resources, disrupting and threatening the balance of ecosystems [4, 5]. The scarcity of water resources in the existing ecosystem, combined with wastes from different sources, has further increased environmental pollution and the aforementioned challenges. Thus, this situation has posed serious risks to both the environment and public health [6, 7]. One of the main causes of water pollution that carries these risks is known to be chemical pollutants, including various industrial dyes widely used in sectors such as textiles, paper, leather and plastics [8, 9]. Especially among these pollutants, dyes in industrial wastewater increase the toxicity of water and cause unpleasant odors and taste. For these reasons, it constitutes an important environmental problem [10, 11]. Around 280,000 tons of the 1.6 million tons of dyes generated annually worldwide are known to find their way into natural water supplies through industrial effluent [12, 13]. Human health, aquatic ecosystems, and biodiversity are all seriously threatened by such environmental releases [14]. In example, the textile sector produces large volumes of wastewater during dyeing processes and uses 100–200 L of water each kilogram of textiles produced. This demonstrates how urgently we need efficient wastewater treatment methods [15]. Wastewater cleanup is becoming more and more necessary every day. Adsorption method has emerged as one of the most effective, efficient and economical methods for the removal

✉ Uğur Özkan
ugurozkan@isparta.edu.tr

Okan Bayram
okan.bayram.32@gmail.com; okanbayram@sdu.edu.tr

Halil Turgut Şahin
halilsahin@isparta.edu.tr

[1] Faculty of Forestry, Department of Forest Products Engineering, Isparta University of Applied Sciences, 32200 Isparta, Türkiye

[2] Faculty of Engineering and Natural Sciences, Department of Chemistry, Süleyman Demirel University, 32200 Isparta, Türkiye

of toxic and persistent pollutants from wastewater as well as for the removal of pollutants resistant to biodegradation. Higher removal efficiency, softer operating conditions, and reduced waste generation are some benefits of the adsorption method over traditional techniques like chemical coagulation, ion exchange, electrolysis, and biological treatment [16–19]. The adsorbent's features, including cost, removal efficiency, resource abundance and ease of engineering, determine how important these benefits are in the adsorption process [20]. To boost adsorbent capacity, scientists have investigated a variety of adsorbent materials in recent years, with encouraging outcomes [21–23]. In this context, considering the criteria such as low cost, sustainability and easy transportation, the cones of *Juniperus Excelsa* (JE), one of the juniper tree species with a wide distribution in Turkey, were selected as adsorbent material for the treatment of malachite green (MG) dye for this study. This natural adsorbent was converted into biochar (JEB) form and then modified with iron (mJEB) to become a magnetic material to increase its adsorption capacity. Biochar is essential in environmental sciences owing to its oxygen-containing functional groups, elevated surface area, substantial cation exchange capacity, and cost-effective alkaline properties [24]. Kul et al. (2019) achieved q_{max} values ranging from 3.060 mg/g to 16.530 mg/g for Basic Blue 41 removal at concentrations ranging from 25 to 100 mg/L [25]. Nikolova et al. (2019) achieved a q_{max} value of 143.000 mg/g in Cr(VI) removal with *Juniperus excelsa* needles [26]. The novelty of this study is that adsorption studies on *Juniperus excelsa* are few in number and *Juniperus excelsa* is accessible and economical. Important sorption parameters such as temperature, concentration, adsorbent dosage, pH and contact time were investigated during the adsorption process. In addition, the adsorbent was characterized by FT-IR, XRD, SEM, pH_{PZC} and BET analyses to better understand its structural properties.

2 Material and methods

2.1 Chemicals and instruments used in experiments

Malachite Green (MG) a ISOLAB® brand cationic dye, was used in the study. JE cones, collected from Isparta, Turkey, were employed as the adsorbent material. Analytical-grade chemical reagents, including MG ($C_{52}H_{54}N_4O_{12}$), $FeCl_3{\cdot}6H_2O$, 0.1 M NaOH, 0.1 M HCl and $FeSO_4{\cdot}7H_2O$, were prepared with ultrapure water to ensure purity. Stock solutions were diluted as needed to prepare experimental solutions with the desired concentrations. Table 1 shows the physicochemical properties of malachite green (MG), the cationic dye investigated in this study. These properties include the chemical structure, molecular weight, formulation and wavelength values of MG. These characteristics is important in understanding how the dye behaves under different environmental conditions and in assessing its potential application areas.

2.2 Biochar (JEB) and modification (mJEB) of *Juniperus Excelsa* Cone

Biochar (JEB) was created by burning the adsorbent material, *Juniperus excelsa* cones, for 4.5 h at 450 °C in a Carbolite ELF 11/6B muffle furnace. Modified with iron was added to this biochar, which was then utilized in adsorption tests (mJEB). After being washed, the cones were kept for a day at room temperature before being dried for another day at 60°C. Figure 1 shows the state of the adsorbent on the tree (a), after collection (b) and after biocharization (c).

The modification procedure involved adding 25 mL of $FeCl_3{\cdot}6H_2O$ and 25 mL of $FeSO_4{\cdot}7H_2O$ solutions to a volumetric flask containing 5 g of dried biosorbent and 100 mL of distilled water. After an hour of stirring at room temperature to fully dissolve the iron salts, biochar was added, and the mixture was agitated for an additional half hour. 30% ammonia solution was added dropwise to the suspension to change its pH. The observed hue shift indicated the production of mJEB. An external magnet was used to extract the mJEB from the solution, which were then cleaned three times with deionized water and dried for 24 h at 50 ℃ [27, 28]. The synthesis scheme is shown in Fig. 2.

2.3 Characterization of mJEB

The materials were characterized using FT-IR analysis within a wavelength range of 4000–400 cm^{-1}. UV-Vis measurements, including wavelength scanning and dye adsorption studies, were conducted using a Peak Instruments C-7100 UV/Vis device. pH measurements were performed

Table 1 Properties of Malachite green (MG) dye

Dye Name	Formula	Weight	λ_{nm}	Structure
MG	$C_{52}H_{54}N_4O_{12}$	927.010 g/mol	617	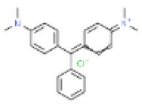



Fig. 1 Various states of JE and JEB

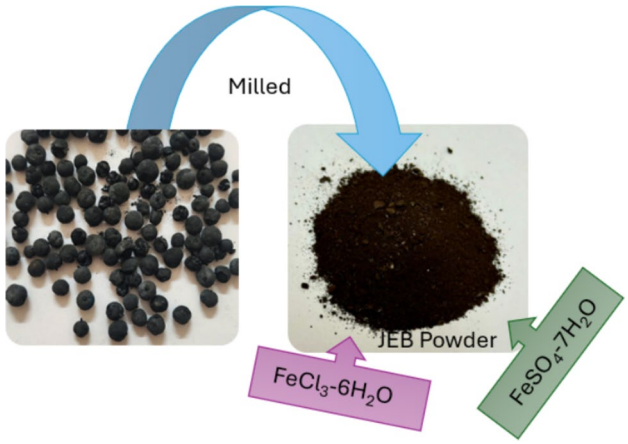

Fig. 2 JEB's modified flow graph

with a Hanna HI2020-02 Edge VR Model pH meter. FT-IR spectroscopy was carried out using a JASCO FT/IR-4700 Type A instrument. SEM analyses were conducted with a Quanta-FEG-250 device, while XRD analysis was performed using a Bruker D8 Advance Twin instrument. Surface area and porosity of the mJEB were determined through Brunauer–Emmett–Teller (BET) analysis with a Micromeritics Gemini VII 2390t brand device.

2.4 MG Removal experiments with mJEB

The *Juniperus excelsa* cone biochar (JEB), selected as the adsorbent, was further modified with iron to produce mJEB. The batch adsorption method employed to remove MG from aqueous solutions using mJEB was consistent with procedures reported in the literature. Various adsorption parameters, including pH, temperature, contact time, initial dye concentration and adsorbent dosage, were analyzed to provide a comprehensive understanding of the interaction between MG and mJEB under different conditions. Experiments were carried out at pH values of 2–11 with contact times ranging from 15 to 240 min, mJEB dosages between 0.05 and 0.45 g, temperatures from 25℃ to 55℃ and initial MG concentrations of 50–300 mg/L [27–29]. The values obtained from the adsorption parameters were calculated with the help of Eq. 1 [30].

$$Qe = \frac{(C_0 - C_e)}{W} xV \tag{1}$$

where C_0, C_e, MG dye concentrations at initial, equilibrium phase and at time t, V is the volume, W is the mJEB mass.

3 Results and discussion

3.1 mJEB Characterization results

3.1.1 BET analysis results

BET analysis is frequently used to assess the porosity and surface area of solid (powder) materials. Using information from the low partial pressure region of the adsorption isotherm, this method calculates the amount of adsorbate required to create a tightly packed monolayer of molecules on the sample's surface. The physical and chemical characteristics of different materials are known to be significantly influenced by surface area and porosity [31–33]. The BET analysis results for mJEB are summarized in Table 2.

The results of BET analysis show that mJEB has an ideal adsorbent potential for MG removal. The specific surface area measured as 212.362 m^2/g provides many active sites for adsorption. t-Plot analysis reveals that micropores make a significant contribution to the total adsorption capacity with a micropore surface area of 133.525 m^2/g and an external surface area of 79.837 m^2/g. The Single Point value was found to be 215.164 m^2/g. In this context, the adsorption–desorption graph of mJEB for MG removal is given in Fig. 3.

Table 2 BET analysis results

	Single point (m^2/g)	BET (m^2/g)	t-plot micropore (m^2/g)	t-Plot external (m^2/g)	BJH adsorption (m^2/g)	Single point adsorption* (cm^3/g)	t-Plot micropore (cm^3/g)	BJH adsorption (cm^3/g)	Adsorption (Å)	Desorption (Å)	BJH adsorption (Å)	BJH desorption (Å)
mJEB	215.164	212.362	132.525	79.837	81.330	0.190	0.065	0.128	35.756	35.756	62.801	73.178

Figure 3 shows the variation of quantity adsorbed depending on the relative pressure. Adsorption and desorption curves represent the adsorption processes under different conditions. The adsorption curve rises as the relative pressure increases and reaches equilibrium at a certain point, forming a plateau. This indicates that adsorption reaches its limit when the active sites on the surface are filled. The difference between the different curves reveals how various conditions (e.g. temperature, pH or adsorbent dosage) affect the adsorption capacity.

3.1.2 XRD analysis results

A popular analytical method for closely analyzing a material's atomic arrangement and crystal structure is X-ray diffraction (XRD). This technique makes it possible to determine the short-range order in non-crystalline (amorphous) materials as well as the long-range order in crystalline materials, which is defined as the regular arrangement of atoms. Lattice constants, phase structures, average grain size, crystallinity and crystal defects are only a few of the important structural characteristics that may be discovered using XRD research [34, 35]. The XRD analysis results for mJEB are presented in Fig. 4.

Figure 4 shows that mJEB contains both amorphous and crystalline structures together. The broad peak seen at low 2θ regions indicates the presence of amorphous structure and that this structure can increase adsorption efficiency by providing active sites with large surface area. The extreme peaks indicate the presence of crystalline phases, contributing to surface stability and selectivity. Especially the prominent peaks between 30°−65° reveal that crystalline structures contribute to the adsorption mechanisms.

3.1.3 FT-IR analysis results

Fourier Transform Infrared Spectroscopy (FT-IR) can determine the molecular composition of a material by analyzing its vibrational spectra. It measures the sample's infrared absorption, reflection, transmission or emission to produce a spectrum that provides details on the chemical structure. FT-IR is particularly effective at identifying and quantifying molecules with functional groups, such as amides, carboxylic acids, and carbon-hydrogen bonds [29, 30, 34, 36]. Complexation reactions with dyes are responsible for the production of these groups. Figure 5 shows the FT-IR spectra for mJEB, which were analyzed at intervals of 4 cm^{-1} throughout a wavelength range of 4000–400 cm^{-1}.

When Fig. 5 is examined; since the 3353.6 cm^{-1} peak is observed broadly, it is evaluated that it represents O–H (hydroxyl group) stretching vibrations. In cases where the 3353.6 cm^{-1} peak is observed narrower, it can also be

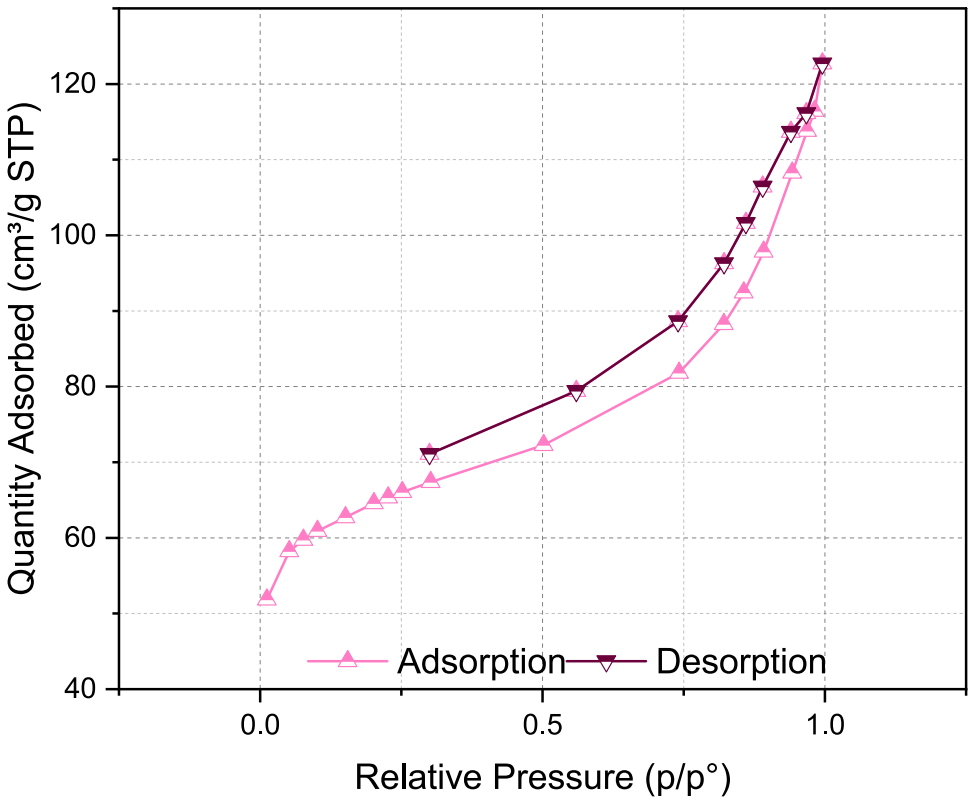

Fig. 3 Adsorption–desorption graph

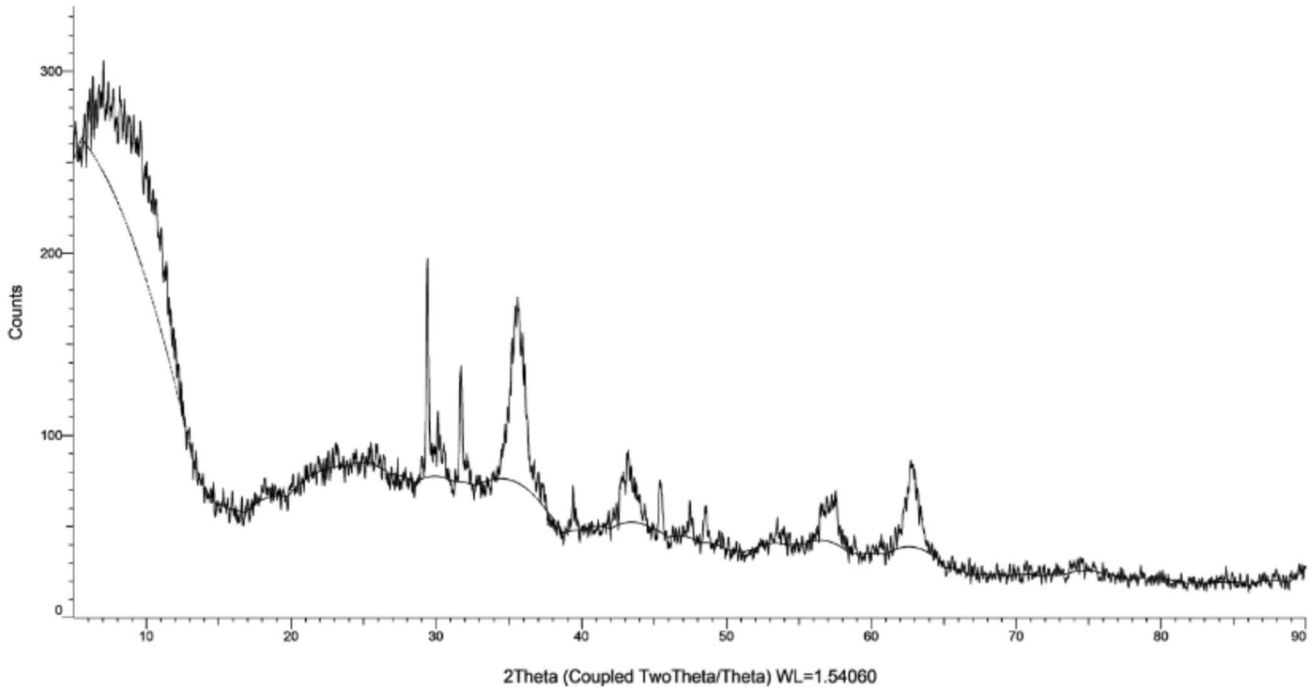

Fig. 4 XRD result graph

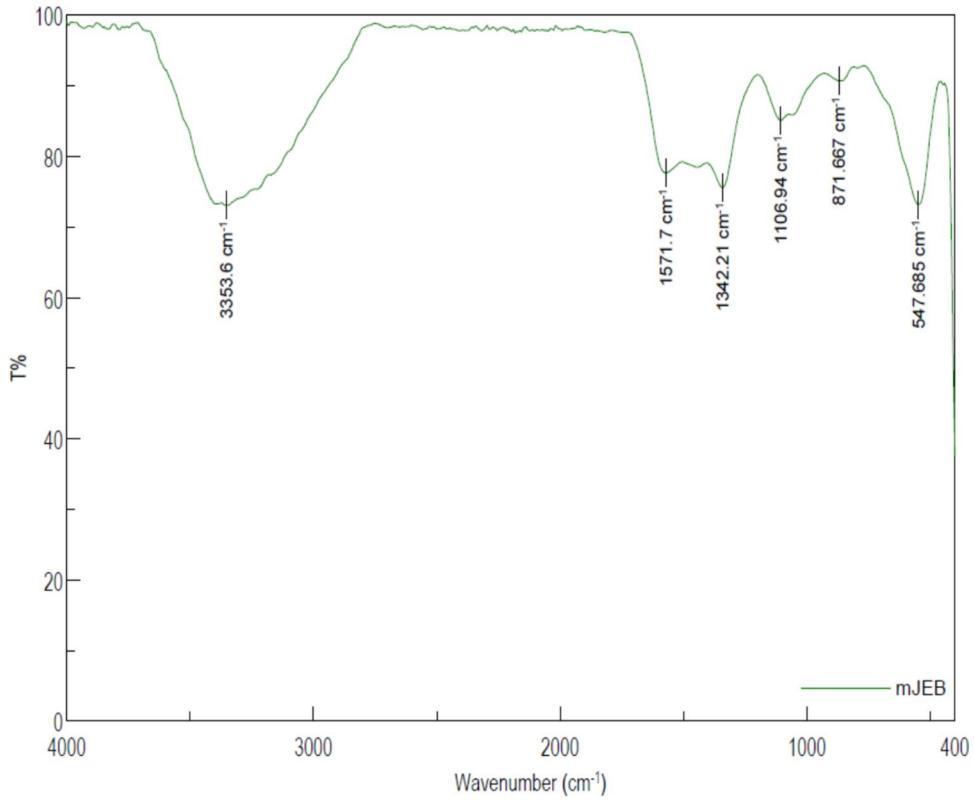

Fig. 5 FT-IR results

evaluated that it represents N–H (amine or amide) stretching [37]. The peak at 1571.7 cm^{-1} is considered to indicate N–H bending [38] C = C (aromatic ring stretching) or C = N (imine or azomethine) vibrations of the amine groups. The peak at 1342.21 cm^{-1} generally indicates C-H bending [39] or asymmetric stretching vibrations of NO_2 (nitro group). The peak at 1106.94 cm^{-1} indicates C-O stretching vibrations [40]. Functional groups containing carbon–oxygen bonds give characteristic peaks in this region. The peak at 871.667 cm^{-1} in the fingerprint region indicates the presence of alkenes and alkyl halides [41]. Peaks at low wavelengths such as 547.685 cm^{-1} generally represent vibrations of heavy atoms. Bonds such as C–Cl, C–Br or C-O [42] can create vibrations in this region.

3.1.4 pH_{PZC} analysis results

pH at which the surface of a solid substance has an equal quantity of positive and negative charges and no net charge is known as the point of zero charge (pH_{PZC}). The mass titration method, which involves weighing the solid and suspending it in a solution with a known pH, can be used to calculate the pH_{PZC}. Changes in the solid's mass are determined by gradually adjusting the pH using a mild acid or base. Until the pH_{PZC} designated by the point of minimal mass change is found, this procedure is repeated. pH_{PZC} plays a crucial role in understanding a material's surface behavior, including its solubility, adsorption and reactivity. While the mass titration method is simple and effective, it requires precise measurement and can be time-consuming [43–45]. Figure 6 is shown the pH_{PZC} results.

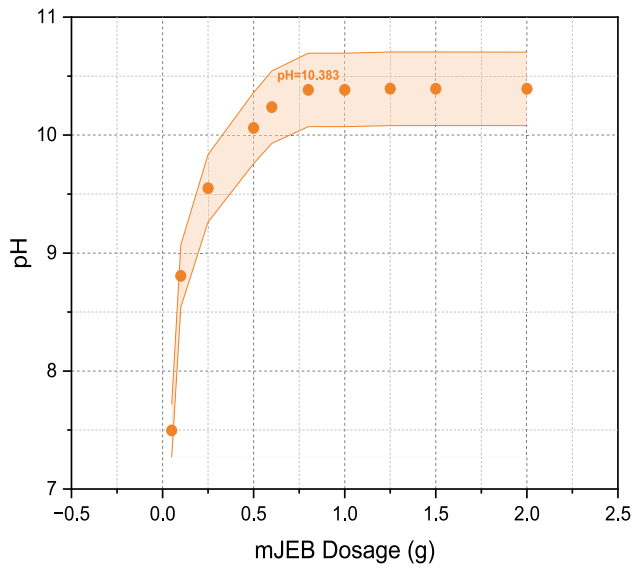

Fig. 6 pH_{PZC} results (conditions: mJEB dosage: 0.05 g, 0.1 g, 0.25 g, 0.5 g, 0.6 g, 0.8 g, 1 g, 1.25 g, 1.5 g, 2 g; solution: 50 mL 0.1 M NaOH)

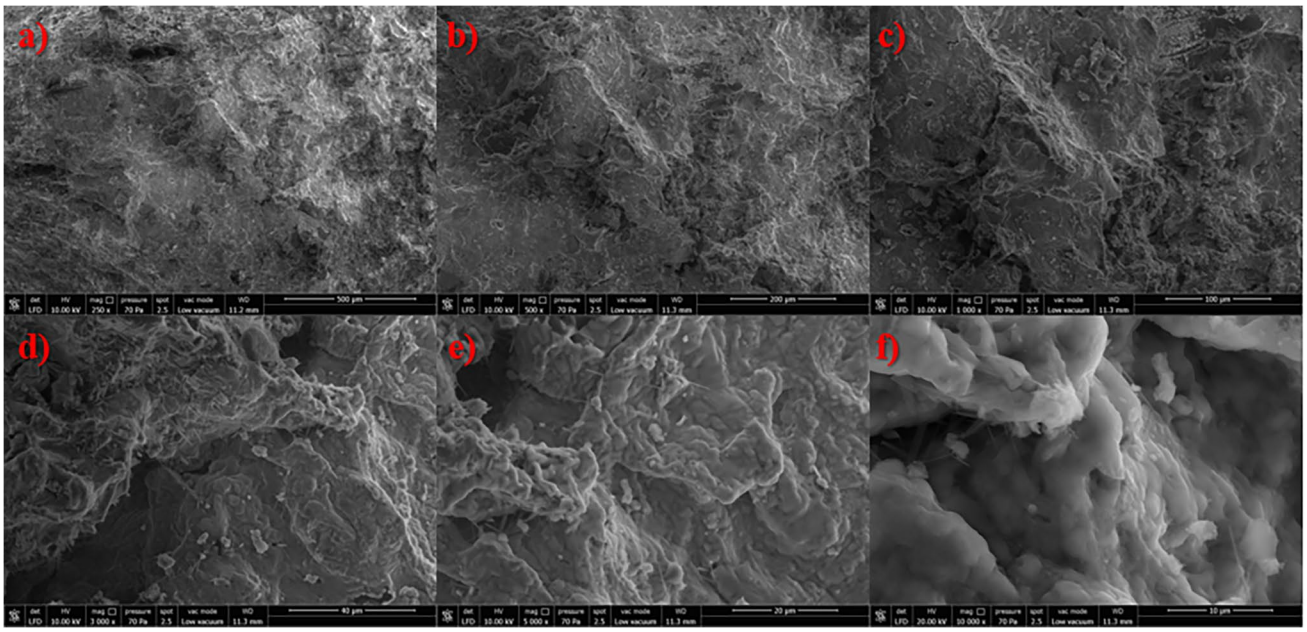

Fig. 7 SEM magnitudes: **a**) 250× **b**) 500× **c**) 1000× **d**) 3000× **e**) 5000× **f**) 10.000×

Figure 6 shows how the surface charge of mJEB adsorbent changes depending on the pH change and the pH_{PZC} value. At the point where the pH value is approximately 10.383, it is seen that the total positive and negative charges of the mJEB surface are balanced, i.e. the surface is neutral. It is seen that the surface charge reaches an equilibrium as the pH and adsorbent dosage increases. This shows that the surface chemistry of the adsorbent changes depending on pH and at different pH levels different ions become suitable for the adsorption mechanism.

3.1.5 SEM analysis results

SEM results for mJEB are shown in Fig. 7.

In Fig. 7, SEM images (Fig. 7a-7f) reveal the surface morphology and structural features of the mJEB adsorbent in detail. The images show that the adsorbent has an irregular, porous and rough surface structure, which provides a large surface area and more active sites, offering a favorable environment for MG adsorption. The presence of pores can facilitate the diffusion of molecules to the surface and increase the adsorption capacity.

3.2 Adsorption parameters experiments results

3.2.1 Effect of mJEB dosage

The efficiency of dye adsorption is significantly impacted by the amount of adsorbent used. While increasing the adsorbent quantity can enhance dye removal, it also raises costs. The optimal amount of adsorbent depends on the specific properties of the dye and adsorbent, as well as the desired outcomes. Generally, a higher adsorbent dosage increases the surface area available for dye adsorption, leading to improved adsorption rates. However, beyond a certain point, further increases may not proportionally enhance dye removal due to limited adsorption sites. Other factors, such as dye concentration, solution pH, and competing compounds, can also influence adsorption efficiency. In some cases, excessive adsorbent may even reduce effectiveness due to site competition or process interference. Therefore, determining the optimal adsorbent dosage requires experimental testing and optimization [46–48]. The impact of varying mJEB dosages is show in Fig. 8.

As the adsorbent dosage increases, the graph shows an increase in adsorption capacity; however, after a while, the capacity increase slows down and reaches the saturation level. While the filling of these sites limits the increase in adsorption capacity at high doses, the quick increase in adsorption capacity at low dosages suggests that there are more active sites available on the adsorbent surface.

3.2.2 Effect of initial pH of MG

From the design of catalytic systems to the treatment of wastewater, adsorption is crucial in many industrial and environmental applications. The pH of the solution is one of the crucial factors that has a major impact on the

adsorption process [49]. Since pH influences the adsorbent's surface characteristics as well as the adsorbate molecules' chemical characteristics, it is one of the most crucial system parameters in adsorption processes. Figure 9 show how MG removal using mJEB is affected by pH changes.

When Fig. 9 is examined, adsorption capacity remains limited at low pH values, but an increase in capacity is observed as pH increases. This increase can be attributed to the effect of pH on the ionization on the adsorbent surface and the ionic form of the target molecule. While the pH level remains partially constant between 6–7, it is seen that it makes a significant peak between 7–8. It is seen that it reaches saturation after pH 8 [49].

3.2.3 Effect of contact time and kinetic studies

Contact time is a factor that influences multiple aspects of the adsorption process and is fundamental for accurate kinetic modeling. Contact time experiments were conducted at intervals of 15–240 min. The results of these experiments are show in Fig. 10.

Figure 10 shows the effect of contact time on the adsorption process of mJEB adsorbent. Initially, a rapid increase in adsorption capacity was observed with the increase in contact time. However, after a certain period of time, the capacity reaches saturation level and no significant increase is observed despite the addition of more contact time. The study of adsorption kinetics is essential for designing efficient adsorption systems. Kinetic models are applied to assess the performance of adsorbents and to understand the mechanisms of mass transfer. Proper interpretation of these models, along with the development of standardized solution methods, is crucial for their practical application [50]. Two commonly used adsorption kinetic models (pseudo-first-order and pseudo-second-order) were used to determine the adsorption rate of mJEB on MG dye. The model results are given in Table 3.

Table 3 compares the kinetic parameters of mJEB adsorbent according to PFO (pseudo-first-order) and PSO (pseudo-second-order) models. The R^2 of the PFO model is 0.878, indicating that the fit of the results is low compared to PSO. The R^2 of PSO was 0.999, indicating a very good fit. These results indicate that the adsorption kinetics of mJEB adsorbent is more suitable for PSO kinetic model [51, 52].

3.2.4 Effect of temperature change and thermodynamic studies

When it comes to dye adsorption on different adsorbents, temperature has a big impact on both thermodynamics and equilibrium. By improving molecular mobility and increasing the frequency of collisions between dye molecules and the adsorbent surface, higher temperatures often accelerate the adsorption rate. Furthermore, by increasing the accessibility of adsorption sites for dye molecules, higher temperatures can increase adsorption capacity. It is a complicated phenomenon, though, as the impact of temperature on adsorption can differ based on the kind of adsorbent, dye, and process variables. Because it affects kinetics, stability, and thermodynamics, temperature plays a significant role in

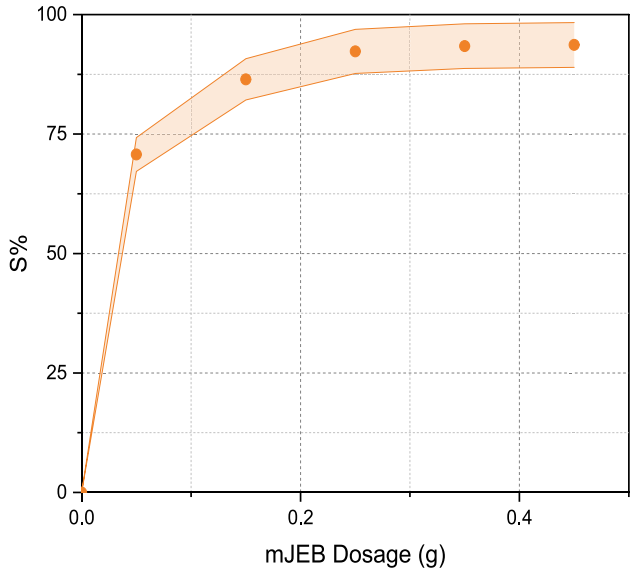

Fig. 8 Effect of mJEB dosage change (conditions: dosage: 0.05 g, 0.15 g, 0.25 g, 0.35 g, 0.45 g; concentration: 100 mg/L MG; temperature: 25 ℃; pH: dye; time: 60 min)

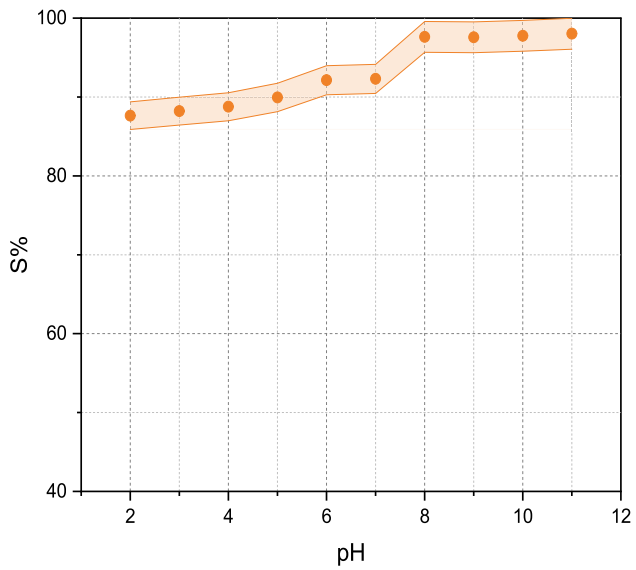

Fig. 9 Effect of pH change (conditions: dosage: 0.25; concentration: 100 mg/L MG; temperature: 25 ℃; pH: 2–11; time: 60 min)

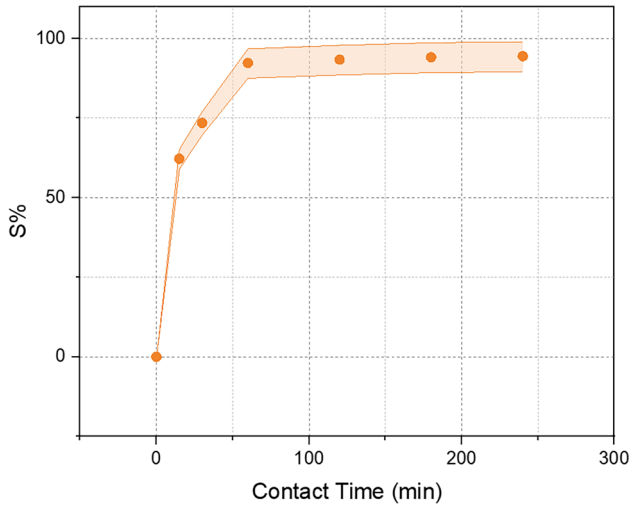

Fig. 10 Effect of contact time change (conditions: dosage: 0.25; concentration: 100 mg/L MG; temperature: 25 ℃; pH: dye; time: 15–240 min)

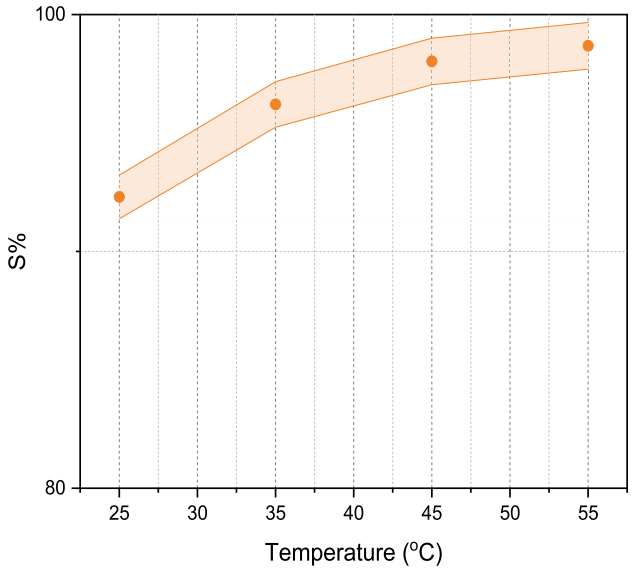

Fig. 11 Effect of temperature change (conditions: dosage: 0.25; concentration: 100 mg/L MG; temperature: 25 ℃−55 ℃; pH: dye; time: 60 min)

adsorption processes [53–55]. Effect of temperature variations (25 ℃, 35 ℃, 45 ℃, 55 ℃) is shown in Fig. 11.

Figure 11 shows the temperature dependence of the performance of mJEB adsorbent in MG removal. The results show that increasing temperature leads to a steady increase in the percentage of MG removal. This show that the adsorption process has an endothermic mechanism and higher temperatures strengthen the interactions between adsorbent and adsorbate. Table 4 shows the increase in temperature from 298.15 to 328.15 and the results of thermodynamic parameters. At T(K) 318.15, ΔG°, ΔS° and ΔH° found −10.324, 189.709, 50.272, respectively.

Table 4 Thermodynamic parameters

T(K)	ΔG° (kJ/mol)	ΔS° (kJ/mol)	ΔH° (kJ/mol)
298.15	–6.157	189.709	50.272
308.15	–8.285		
318.15	–10.324		
328.15	–11.773		

3.2.5 Effect of initial MG concentration and isotherm studies

Dye concentration in the solution is a crucial factor affecting its adsorption onto an adsorbent. Higher dye concentrations increase the number of dye molecules in solution, leading to greater adsorption due to more frequent collisions with the adsorbent surface. However, as the dye concentration rises, the adsorption rate may decrease, particularly at higher saturation levels. The adsorption capacity of the adsorbent also increases with higher dye concentrations, enhancing

Table 3 Kinetic parameters results

Kinetic Model	$q_{e\text{-}cal}$ (mg/g)	k_1	k_2(g/mg. min.)	$q_{e\text{-}exp.}$ (mg/g)	R^2
PFO	5.140	0.000334	-	11.900	0.878
PSO	12.468	–	0.008510	11.900	0.999

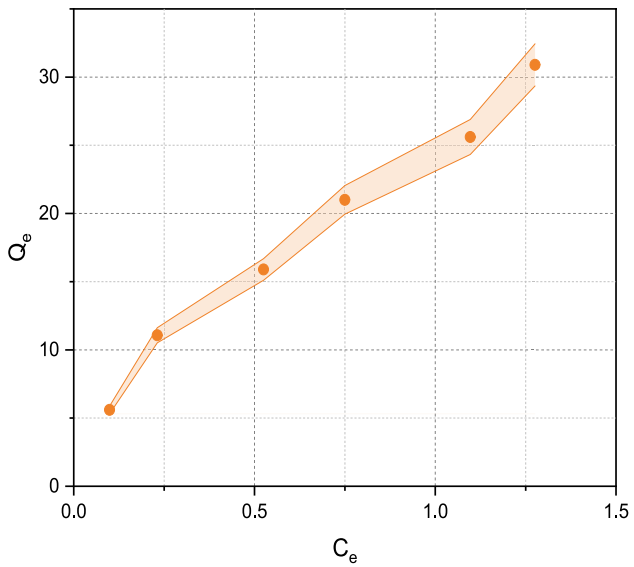

Fig. 12 Effect of concentration change (conditions: dosage: 0.25; concentration: 50–300 mg/L MG; temperature: 25 ℃; pH: dye; time: 60 min)

Table 5 Isotherm parameters results

Isotherm models	Parameters for dye			
Langmuir [59]	q_{max}	K_L	R^2	R_L
	38.023	1.741	0.993	0.011
Freundlich [60]	K_f	1/n	R^2	
	25.264	0.632	0.990	
Temkin & Pyzhev [61]	BT	K_t	R^2	
	9.174	15.316	0.934	
Dubinin&Radushkevich [62]	Q_m	β	R^2	
	3.421	3×10^{-8}	0.990	
Scathard [63]	Ks	Qs	R^2	
	1.357	44.176	0.847	

the likelihood of interaction between dye molecules and adsorption sites. Dye concentration influences the adsorption process's capacity, rate, and equilibrium state, making it a key parameter to consider [56–58]. The effect of MG dye concentration variation is shown in Fig. 12.

Adsorption isotherms are mathematical models that describe the adsorption behavior of molecules on solid surfaces. The adsorbent material, mJEB, was found to be more suitable for MG removal than the Langmuir isotherm model. K_L, R^2 and R_L values were 1.741, 0.993, 0.011, respectively. Langmuir isotherm assumes that the surface is homogeneous and adsorption is monolayer. The isotherm parameter results calculated in the study are given in Table 5.

The maximum adsorption capacity (q_{max}) value of mJEB in MG removal was found to be 38.023 mg/g. Comparison with studies in the literature on MG removal with biochars is given in Table 6.

3.2.6 mJEB recycling study

Recycling study was carried out with 0.1 mol/L HCl using the method we explained in our previous study [73]. The results obtained by investigating the reusability of mJEB in MG removal are given in Fig. 13. In the experiments carried out in three cycles, mJEB reached 92.301%, 85.753%, 76.392% removal percentages, respectively. This shows that mJEB can be reused in MG removal. In their study, Ahmad et al. (2025) achieved 95.710%, 95.600%, 95.550%, 94.860%, 82.550% removal percentages in five cycles in MG removal with MgAlLDH@Fe_3O_4 [74]. In their study conducted by Su et al. (2025), they achieved 97.700%, 92.600%, 88.500%, 86.780%, 82.300% removal percentages in five cycles for MG removal with 1ZnAl-LDO@BC [75]. Here, even though mJEB reaches lower values in cycles, it stands out with its economy and accessibility.

3.2.7 Adsorption mechanism of mJEB

In this study, the adsorption of MG by mJEB was evaluated to occur through various interaction mechanisms. The possible different mechanisms involved in the adsorption process are shown in Fig. 14. It is considered that these mechanisms contributing to the removal of MG may include different types of interactions such as hydrogen bonding, electrostatic interactions [76], and π-π interactions [77, 78]. In addition, it is considered that a specific interaction occurs between MG molecules and iron particles. Various possible interactions between MG and these chemical groups may take place on the surface of mJEB [77]. It is evaluated that as the pH increases, the functional groups of the adsorbent gain a negative charge, which attracts the cationic MG dye

Table 6 Studies on MG removal in the literature

Adsorbent	Q_{max} (mg/g)	References
PBB *(Pinus brutia)*	13.004	[27]
nM-PBB *(nM-Pinus brutia)*	18.215	[27]
Cassava peel carbon (CPC)	282.640	[64]
RSW500 *(reed straw waste)*	185.350	[65]
Opuntia Ficus-indica activated carbon	200.100	[66]
Soybean meal biochar	189.990	[67]
RHMB *(Rice husk derived biochar modified)*	373.020	[68]
Biochar-supported nano zero-valent iron composite	909.090	[69]
Magnetic biochar from sewage sludge	388.650	[70]
0.3 SnO_2-SBB *(SnO_2-modified sugarcane bagasse biochar nanocomposites)*	52.640	[71]
0.5 SnO_2-SBB *(SnO_2-modified sugarcane bagasse biochar nanocomposites)*	73.860	[71]
MnO_2-NP-CPC	319.40	[72]
mJEB	38.023	**This study**

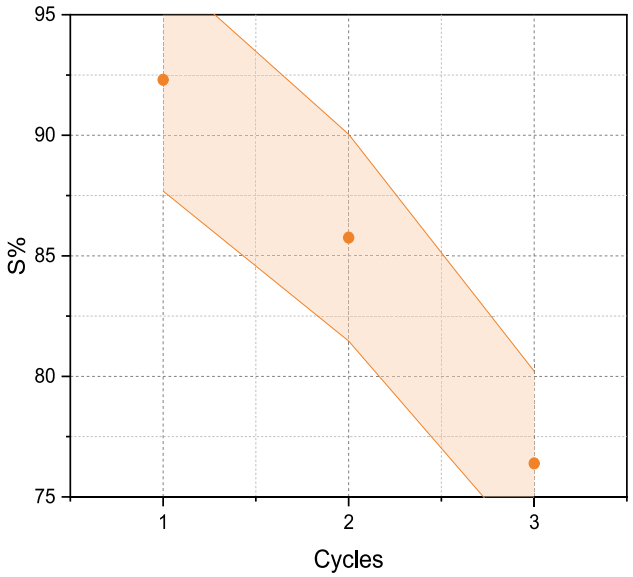

Fig. 13 Cycles experiments (conditions: dosage: 0.25; concentration: 100 mg/L MG; temperature: 25 ℃; pH: dye; time: 60 min)

with positively charged (-+N(CH) group) using electrostatic interactions [78]. Electrostatic attraction may occur as a result of interactions between the negatively charged functional groups on the surface and MG. Additionally, complexation between Fe^{3+} ions on the surface and MG may contribute to the adsorption process. Furthermore, the aromatic structure of MG is considered to support the adsorption process through π-π interactions with π-π electron on the biochar surface. The pore-filling mechanism may also enhance the adsorption capacity by physically trapping MG molecules within the pores of the biochar structure [77, 78]. The influence of these interactions enhances the efficiency of the adsorption process, indicating that mJEB is an effective alternative for MG removal.

4 Conclusion

Pollution of clean water resources in the world constitutes a significant environmental problem. Pollution of clean water resources with dyes and mixing of these wastewaters with clean waters without treatment is a major problem. In this study, mJEB was produced from JE considering accessibility and production cost. MG, a cationic dye, was removed from aqueous solutions with mJEB. In experiments conducted with the batch adsorption method, it was found that the process proceeded via PSO, was endothermic, and complied with the Langmuir isotherm model. $q_{max} = 38.023$ mg/g was found in MG removal with mJEB. It is evaluated that mJEB can be preferred in MG removal because it is natural and economical. In addition, the fact that there are few dye removal studies with JE in the literature makes this study important and focuses on the investigation of this subject.

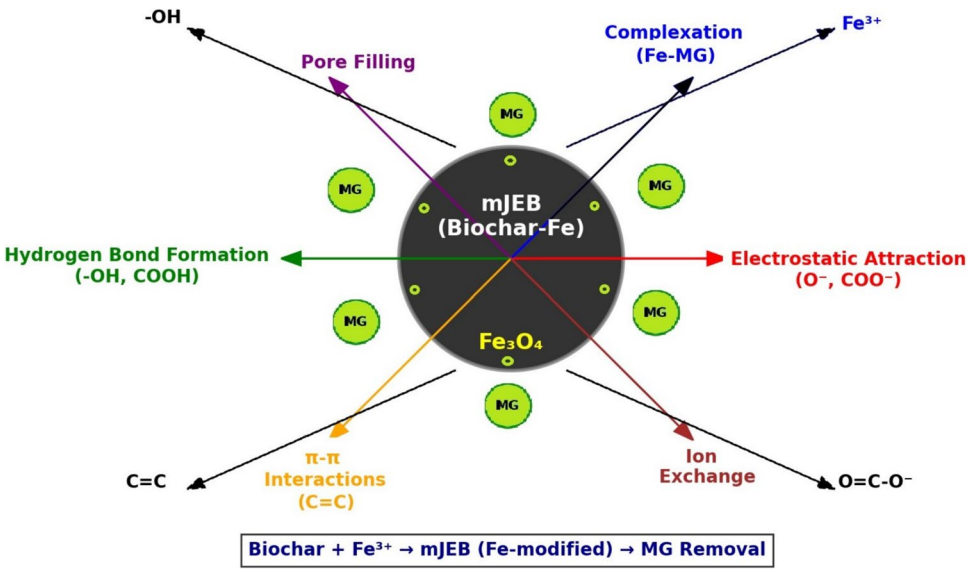

Fig. 14 Adsorption mechanism of mJEB

Author contributions Uğur Özkan: Methodology, Investigation, Writing – review & editing original draft, Data curation, Conceptualization, Validation. Okan Bayram: Methodology, Investigation, Data curation, Validation, Conceptualization, Methodology, Test, Writing – review & editing original draft. Halil Turgut Şahin: Conceptualization, Project administration.

Funding Open access funding provided by the Scientific and Technological Research Council of Türkiye (TÜBİTAK). Open access funding provided by the Scientifc and Technological Research Council of Türkiye (TÜBİTAK).

Data availability Data will be available on reasonable request.

Declarations

Ethics approval Not applicable.

Informed consent All authors agree to this publication.

Competing interests The authors have no competing interests to declare that are relevant to the content of this article.

Open Access This article is licensed under a Creative Commons Attribution 4.0 International License, which permits use, sharing, adaptation, distribution and reproduction in any medium or format, as long as you give appropriate credit to the original author(s) and the source, provide a link to the Creative Commons licence, and indicate if changes were made. The images or other third party material in this article are included in the article's Creative Commons licence, unless indicated otherwise in a credit line to the material. If material is not included in the article's Creative Commons licence and your intended use is not permitted by statutory regulation or exceeds the permitted use, you will need to obtain permission directly from the copyright holder. To view a copy of this licence, visit http://creativecommons.org/licenses/by/4.0/.

References

1. Zamora-Ledezma C, Negrete-Bolagay D, Figueroa F, Zamora-Ledezma E, Ni M, Alexis F, Guerrero VH (2021) Heavy metal water pollution: A fresh look about hazards, novel and conventional remediation methods. Environ Tech Innov 22:101504. https://doi.org/10.1016/j.eti.2021.101504
2. Noor R, Maqsood A, Baig A, Pande CB, Zahra SM, Saad A, Anwar M, Singh SK (2023) A comprehensive review on water pollution. South Asia Region: Pakistan Urban Clim 48:101413. https://doi.org/10.1016/j.uclim.2023.101413
3. Assouani A, Dabagh A, Abali M, Mahmoudy G, El-Habacha M, Chiban M, Alahiane N, Fdil F, Sinan F, Zerbet M (2024) Evaluation of the physicochemical and bacteriological quality of groundwater in the Nihit rural commune of the Moroccan Anti-Atlas. Des Water Treat 317:100038. https://doi.org/10.1016/j.dwt.2024.100038
4. Iaich S, Miyah Y, Elazhar F, Lagdali S, El-Habacha M (2021) Low-cost ceramic microfiltration membranes made from Moroccan clay for domestic wastewater and Congo Red dye treatment. DWT 235:251–271. https://doi.org/10.5004/dwt.2021.27618
5. Thongsamer T, Vinitnantharat S, Pinisakul A, Werner D (2023) Fixed-bed biofilter for polluted surface water treatment using chitosan impregnated-coconut husk biochar. Environ Pollut 334:122137. https://doi.org/10.1016/j.envpol.2023.122137
6. Şenol ZM, El Messaoudi N, Cigeroglu Z, Miyah Y, Arslanoglu H, Baglam N, Kazan-Kaya ES, Kaur P, Georgin J (2024) Removal of food dyes using biological materials via adsorption: a review. Food Chem 450:139398. https://doi.org/10.1016/j.foodchem.2024.139398
7. Chen Z, Wu G, Wu Y, Wu Q, Shi Q, Ngo HH, Vargas Saucedo OA, Hu HY (2020) Water Eco-Nexus Cycle System (Water-EcoNet) as a key solution for water shortage and water environment problems in urban areas. Water Cycle 1:71–77. https://doi.org/10.1016/j.watcyc.2020.05.004
8. Mahmoodi NM, Oveisi M, Taghizadeh A, Taghizadeh M (2020) Synthesis of pearl necklace-like ZIF-8@ chitosan/PVA nanofiber with synergistic effect for recycling aqueous dye removal. Carbohy Poly 227:115364. https://doi.org/10.1016/j.carbpol.2019.115364
9. Liu Z (2021) Xing K (2021) Removal of acid red 88 using activated carbon produced from pomelo peels by KOH activation: orthogonal experiment isotherm and kinetic studies. Journ Chem 1:6617934. https://doi.org/10.1155/2021/6617934
10. Islam Tarekul Repon MR, Islam Tarikul Sarwar Z, Rahman MM (2023) Impact of textile dyes on health and ecosystem: a review of structure, causes, and potential solutions. Environ Sci Pollut Res 30:9207–9242. https://doi.org/10.1007/s11356-022-24398-3
11. Tomar T, Kahandawala N, Kaur J, Thounaojam L, Choudhary I, Bera S (2023) Bioremediation of synthetic dyes from wastewater by using microbial nanocomposites: an emerging field for water pollution management. Biocatal Agric Biotechnol 51:102767. https://doi.org/10.1016/j.bcab.2023.102767
12. Sarma GK, Sen Gupta S, Bhattacharyya KG (2019) Removal of hazardous basic dyes from aqueous solution by adsorption onto kaolinite and acid-treated kaolinite: kinetics, isotherm and mechanistic study. SN App Sci 1:1–15. https://doi.org/10.1007/s42452-019-0216-y
13. Arunprasath T, Sudalai S, Meenatchi R, Jeyavishnu K, Arumugam A (2019) Biodegradation of triphenylmethane dye malachite green by a newly isolated fungus strain. Biocatal Agric Biotechnol 17:672–679. https://doi.org/10.1016/j.bcab.2019.01.030
14. Maiti P, Siddiqi H, Kumari U, Chatterjee A, Meikap BC (2023) Adsorptive remediation of azo dye contaminated wastewater by $ZnCl_2$ modified bio-adsorbent: Batch study and life cycle assessment. Powder Technol 415:118153. https://doi.org/10.1016/j.powtec.2022.118153
15. Tarekegn MM, Balakrishnan RM, Hiruy AM, Dekebo AH (2021) Removal of methylene blue dye using nano zerovalent iron, nanoclay and iron impregnated nanoclay A comparative study. RSC Adv 11(48):30109–30131. https://doi.org/10.1039/D1RA03918K
16. Song Y, Peng R, Gou L, Ye M (2021) Removal of sunset yellow by methanol modified walnut shell. Iran J Chem Chem Eng 40(4):1095–1104. https://doi.org/10.30492/IJCCE.2020.101424.3429
17. Kumar A, Patra C, Rajendran HK, Narayanasamy S (2022) Activated carbon-chitosan based adsorbent for the efficient removal of the emerging contaminant diclofenac: synthesis, characterization and phytotoxicity studies. Chemosphere 307(2):135806. https://doi.org/10.1016/j.chemosphere.2022.135806
18. Priyan VV, Narayanasamy S (2022) Effective removal of pharmaceutical contaminants ibuprofen and sulfamethoxazole from water by corn starch nanoparticles: an ecotoxicological assessment. Environ Toxicol Pharmacol 94:103930. https://doi.org/10.1016/j.etap.2022.103930
19. Farki NN, Abdulhameed AS, Surip AN, ALOthman ZA, Jawad AH (2023) Tropical fruit wastes including durian seeds and rambutan peels as a precursor for producing activated carbon using H_3PO_4-assisted microwave method: RSM-BBD optimization and

mechanism for methylene blue dye adsorption. Int J Phytoremed 25:1–12. https://doi.org/10.1080/15226514.2023.2175780
20. Anfar Z, Zbair M, Ahsaine HA, Ezahri M, Alem NE (2018) Well-designed WO_3/Activated carbon composite for Rhodamine B Removal: Synthesis, characterization, and modeling using response surface methodology. Full Nano Car Nanostruc 26(6):389–397. https://doi.org/10.1080/1536383X.2018.1440386
21. Ahmed MJ, Okoye PU, Hummadi EH, Hameed BH (2019) High-performance porous biochar from the pyrolysis of natural and renewable seaweed (Gelidiella acerosa) and its application for the adsorption of methylene blue. Biores Technol 278:159–164. https://doi.org/10.1016/j.biortech.2019.01.054
22. Mouni L, Belkhiri L, Bollinger JC, Bouzaza A, Assadi A, Tirri A, Dahmoune F, Madani K, Remini H (2018) Removal of Methylene Blue from aqueous solutions by adsorption on Kaolin: Kinetic and equilibrium studies. Appl Clay Sci 153:38–45. https://doi.org/10.1016/j.clay.2017.11.034
23. Sabarinathan C, Karuppasamy P, Vijayakumar CT, Arumuganathan T (2019) Development of methylene blue removal methodology by adsorption using molecular polyoxometalate: Kinetics, Thermodynamics and Mechanistic Study. Microchem Journal 146:315–326. https://doi.org/10.1016/j.microc.2019.01.015
24. Sharma P, Sharma S, Sharma SK, Jain A, Shrivastava K (2024) Review on recent advancement of adsorption potential of sugarcane bagasse biochar in wastewater treatment. Chem Eng Res Des 206:428–439. https://doi.org/10.1016/j.cherd.2024.04.055
25. Kul AR, Aldemir A, Alkan S, Elik H, Çalışkan M (2019) Adsorption of Basic Blue 41 using Juniperus excelsa: Isotherm kinetics and thermodynamics studies. Environ Res Technol 2(3):112–121. https://doi.org/10.35208/ert.568992
26. Nikolova MI, Prokopov TV, Stankov SS, Bozadzhiev BV, Stoyanova AS (2021) Application of biomass from Greek juniper needles (Juniperus excelsa M. Bieb) for removal of Cr (VI) from aqueous solution. IOP Conf Ser Mater Sci Eng 1031:1–012096. https://doi.org/10.1088/1757-899X/1031/1/012096
27. Bayram O, Özkan U, Şahin HT, Göde F (2024) Malachite green (cationic dye) removal with modified Pinus brutia biochar. Inter J Phytorem 26(3):416–426. https://doi.org/10.1080/15226514.2023.2246573
28. Bayram O, Moral E, Pekgözlü İ, Göde F (2024) Use of $Sr_2Mg(BO_3)_2$ in Congo red removal from aqueous solutions: Synthesis, adsorption, isotherm, kinetic study. J Disp Sci Technol 46(1):98–107. https://doi.org/10.1080/01932691.2023.2278497
29. Bayram O, Moral E, Göde F (2023) Removal of Crystal Violet Dye from Aqueous Solution Using Biochar Obtained from Oleaster Seeds. J Instit Sci Technol 13(1):448–457. https://doi.org/10.21597/jist.1170769
30. Belcaid A, Beakou BH, Bouhsina S, Anouar A (2024) Biosorption of cobalt and chromium from wastewater using manganese dioxide and iron oxide nanoparticles loaded on cellulose-based biochar: Modeling and optimization with machine learning (artificial neural network). Int J Biol Macromol 282:136855. https://doi.org/10.1016/j.ijbiomac.2024.136855
31. Odler I (2003) The BET-specific surface area of hydrated Portland cement and related materials. Cement Conc Res 33(12):2049–2056. https://doi.org/10.1016/S0008-8846(03)00225-4
32. Patel S, Orlov A, Ariyachandra E, Peethamparan S (2021) Effect of flue gas temperature on NO_2 adsorption by aged recycled concrete Waste: DRIFTS, TGA and BET study. Chem Eng J 420:130413. https://doi.org/10.1016/j.cej.2021.130413
33. Ahmed A, Pervaiz E, Ahmed I, Noor T (2024) Remarkable Improvement in Drilling Fluid Properties with Graphitic-Carbon Nitride for enhanced Wellbore Stability. Heliyon 11:e41237. https://doi.org/10.1016/j.heliyon.2024.e41237
34. Ikhtiyarova GA, Özcan AS, Gök Ö, Özcan A (2012) Characterization of natural-and organo-bentonite by XRD, SEM, FT-IR and thermal analysis techniques and its adsorption behaviour in aqueous solutions. Clay Miner 47(1):31–44. https://doi.org/10.1180/claymin.2012.047.1.31
35. Khan H, Yerramilli AS, D'Oliveira A, Alford TL, Boffito DC, Patience GS (2020) Experimental methods in chemical engineering: X-ray diffraction spectroscopy XRD. The Can J Chem Eng 98(6):1255–1266. https://doi.org/10.1002/cjce.23747
36. Rather LJ, Mohammad F, Shahid S (2015) Study on the application of Acacia nilotica natural dye to wool using fluorescence and FT-IR spectroscopy. Fibers Polym 16(7):1497–1505. https://doi.org/10.1007/s12221-015-4879-8
37. El-Sakhawy M, Salama A, Kamel S, Tohamy HAS (2018) Carboxymethyl cellulose esters as stabilizers for hydrophobic drugs in aqueous medium. Cellul Chem Technol 52(9–10):749–757
38. Qi P, Zhang T, Shao J, Yang B, Fei T, Wang R (2019) A QCM humidity sensor constructed by graphene quantum dots and chitosan composites. Sens Act A Phys 287:93–101. https://doi.org/10.1016/j.sna.2019.01.009
39. Nandgude TD, Bhise KS, Gupta VB (2008) Characterization of hydrochloride and tannate salts of diphenhydramine. Indian J Phar Sci 70(4):482. https://doi.org/10.4103/0250-474X.44598
40. Sarı A, Hekimoğlu G, Tyagi VV, Sharma RK (2020) Evaluation of pumice for development of low-cost and energy-efficient composite phase change materials and lab-scale thermoregulation performances of its cementitious plasters. Energy 207:118242. https://doi.org/10.1016/j.energy.2020.118242
41. Swathilakshmi AV, Poonkothai M (2024) Ecofriendly Approach on the Removal of Reactive Orange 107 from Aqueous Solutions Using Cladophora Species as a Novel Biosorbent. Molec Biotechnol 66(3):500–516. https://doi.org/10.1007/s12033-023-00764-5
42. Saleh B, Farooqui M, Yusuf S (2021) Cobalt oxide nanoparticles: synthesis and their adsorption study. J Sci Technol (JST) 6(4):69–83. https://doi.org/10.46243/jst.2021.v6.i4.pp69-83
43. Yun TY, Chandler BD (2023) Surface hydroxyl chemistry of titania-and alumina-based supports: quantitative titration and temperature dependence of surface brønsted acid–base parameters. ACS Appl Mater Interfaces 15(5):6868–6876. https://doi.org/10.1021/acsami.2c20370
44. Rubangakene NO, Elwardany A, Fujii M, Sekiguchi H, Elkady M, Shokry H (2023) Biosorption of Congo Red dye from aqueous solutions using pristine biochar and ZnO biochar from green pea peels. Chem Eng Res Des 189:636–651. https://doi.org/10.1016/j.cherd.2022.12.003
45. Zein R, Satrio Purnomo J, Ramadhani P, Safni Alif MF, Putri CN (2023) Enhancing sorption capacity of methylene blue dye using solid waste of lemongrass biosorbent by modification method. Arabian J Chem 16(2):104480. https://doi.org/10.1016/j.arabjc.2022.104480
46. Hameed BH, Mahmoud DK, Ahmad AL (2008) Equilibrium modeling and kinetic studies on the adsorption of basic dye by a low-cost adsorbent: coconut (Cocos nucifera) bunch waste. J Hazard Mater 158(1):65–72. https://doi.org/10.1016/j.jhazmat.2008.01.034
47. Kushwaha P, Agarwal M (2023) Utilization of metal industry solid waste as an adsorbent for adsorption of anionic and cationic dyes from aqueous solution through the batch and continuous study. Environ Sci Pollut Res 30(16):46748–46765. https://doi.org/10.1007/s11356-023-25531-6
48. Kim SH, Kim DS, Moradi H, Chang YY, Yang JK (2023) Highly porous biobased graphene-like carbon adsorbent for dye removal: preparation, adsorption mechanisms and optimization. J Environ Chem Eng 11(2):109278. https://doi.org/10.1016/j.jece.2023.109278
49. Khulbe KC, Matsuura T (2018) Removal of heavy metals and pollutants by membrane adsorption techniques. Appl Wat Sci 8:1–30. https://doi.org/10.1007/s13201-018-0661-6

50. Wang J, Guo X (2020) Adsorption isotherm models: Classification, physical meaning, application and solving method. Chemosphere 258:127279. https://doi.org/10.1016/j.chemosphere.2020.127279
51. Ighalo JO, Iwuozor KO, Igwegbe CA, Adeniyi AG (2021) Verification of pore size effect on aqueous-phase adsorption kinetics: A case study of methylene blue. Coll Sur A Physicochem Eng Asp 626:127119. https://doi.org/10.1016/j.colsurfa.2021.127119
52. Revellame ED, Fortela DL, Sharp W, Hernandez R, Zappi ME (2020) Adsorption kinetic modeling using pseudo-first order and pseudo-second order rate laws: A review. Clean Eng Technol 1:100032. https://doi.org/10.1016/j.clet.2020.100032
53. Mogharbel RT, Alkhamis K, Felaly R, El-Desouky MG, El-Bindary AA, El-Metwaly NM, El-Bindary MA (2023) Superior adsorption and removal of industrial dye from aqueous solution via magnetic silver metal organic framework nanocomposite. Environ Technol 45(13):2558–2574. https://doi.org/10.1080/09593330.2023.2178331
54. Loutfi M, Mariouch R, Mariouch I, Belfaquir M, ElYoubi MS (2023) Adsorption of methylene blue dye from aqueous solutions onto natural clay: equilibrium and kinetic studies. Mater Today proc 72:3638–3643. https://doi.org/10.1016/j.matpr.2022.08.412
55. Sellaoui L, Bouzidi M, Franco DS, Alshammari AS, Gandouzi M, Georgin J, Mohamed NBH, Erto A, Badawi M (2023) Exploitation of Bauhinia forficata residual fruit powder for the adsorption of cationic dyes. J Chem Eng 456:141033. https://doi.org/10.1016/j.cej.2022.141033
56. Borgohain X, Das E, Rashid MH (2023) Facile synthesis of CeO2 nanoparticles for enhanced removal of malachite green dye from an aqueous environment. Mater Adv 4(2):683–693. https://doi.org/10.1039/D2MA01019D
57. Wattanasiriwech S, Naradisorn M, Wattanasiriwech D (2023) Adsorption of the malachite green dye of macadamia husk-activated carbon prepared using a household pyrolysis kiln. Green Mater 11(3):137–144. https://doi.org/10.1680/jgrma.22.00096
58. Vinayagam R, Kandati S, Murugesan G, Goveas LC, Baliga A, Pai S, Varadavenkatesan T, Kaviyarasu K, Selvaraj R (2023) Bioinspiration synthesis of hydroxyapatite nanoparticles using eggshells as a calcium source: evaluation of Congo red dye adsorption potential. J Mater Res Technol 22:169–180. https://doi.org/10.1016/j.jmrt.2022.11.093
59. Langmuir I (1916) The constitution and fundamental properties of solids and liquids. Part I. Solids J American Chem Soci 38:2221–2295
60. Freundlich H (1907) Über die adsorption in lösungen. Z Phys Chem 57:385–470
61. Temkin MJ, Pyzhev V (1940) Recent modifications to Langmuir isotherms. Acta Physiochim USSR 12:217–222
62. Dubinin MM, Radushkevich LV (1947) Equation of the characteristic curve of activated charcoal. Proc Acad Sci USSR Phys Chem Sect 55:331–333
63. Scatchard GD (1949) The attractions of proteins for small molecules and ions. Ann NY Acad Sci 51:660–672
64. Belcaid A, Beakou BH, Bouhsina S, Anouar A (2024) Insight into adsorptive removal of methylene blue, malachite green, and rhodamine B dyes by cassava peel biochar (Manihot esculenta Crantz) in single, binary, and ternary systems: competitive adsorption study and theoretical calculations. Bio Conver Bioref 14(6):7783–7806. https://doi.org/10.1007/s13399-022-02928-w
65. Chen L, Wang H, Tu Z, Hu J, Wu F (2024) Renewable fuel and value-added chemicals potential of reed straw waste (RSW) by pyrolysis: Kinetics thermodynamics, products characterization, and biochar application for malachite green removal. Renew Energy 229:120724. https://doi.org/10.1016/j.renene.2024.120724
66. Belhajjia C, Abid A, Msaad A, Labaali Z, Zouhri A (2021) Synthesis, characterization and adsorption of malachite green dye using novel materiel produced from Opuntia Ficus Indica. Mater Today Proc 37:4001–4006. https://doi.org/10.1016/j.matpr.2020.11.576
67. Falah FZ, Anouar I, Elkouali MH, Bouamrani ML, Yousfi S (2024) Investigation of the removal of malachite green by soybean meal biochar: characterization, modelling, and adsorption mechanism. Int J Envir Analy Chem 14:1–21. https://doi.org/10.1080/03067319.2024.2365773
68. Tsai CY, Lin PY, Hsieh SL, Kirankumar R, Patel AK, Singhania RR, Dong CD, Hsieh CCW, S, (2022) Engineered mesoporous biochar derived from rice husk for efficient removal of malachite green from wastewaters. Biores Technol 347:126749. https://doi.org/10.1016/j.biortech.2022.126749
69. Yıldırım GM, Bayrak B (2022) The synthesis of biochar-supported nano zero-valent iron composite and its adsorption performance in removal of malachite green. Bio Conver Bioref 12(10):4785–4797. https://doi.org/10.1007/s13399-021-01501-1
70. Zhang J, Liu M, Yang T, Yang K, Wang H (2016) A novel magnetic biochar from sewage sludge: synthesis and its application for the removal of malachite green from wastewater. Wat Sci Technol 74(8):1971–1979. https://doi.org/10.2166/wst.2016.386
71. Sharma P, Sharma S, Sharma SK, Yifei S, Guo F, Ichikawa T, Jain A, Shrivastava K (2024) Evaluation of optimized conditions for the adsorption of malachite green by SnO_2-modified sugarcane bagasse biochar nanocomposites. RSC Adv 14(40):29201–29214. https://doi.org/10.1039/D4RA05442C
72. Belcaid A, Beakou BH, Bouhsina S, Anouar A (2023) New insights on manganese dioxide nanoparticles loaded on cellulose-based biochar of cassava peel for the adsorption of three cationic dyes from wastewater. Int J Biol Macromol 241:124534. https://doi.org/10.1016/j.ijbiomac.2023.124534
73. Bayram O, Özkan U, Kardeş S, Moral E, Göde F, Pehlivan E (2025) Sustainable decolorization of methyl blue and malachite green from an aqueous environment using magnetic biochar prepared from the fruit seeds of Mespilus germanica L. Chem Ecol 1:1–24. https://doi.org/10.1080/02757540.2024.2447582
74. Ahmad N, Kameda T, Rahman MT, Lesbani A (2025) Application and regeneration of magnetic material MgAlLDH@Fe_3O_4 humic acid with removal capacity for malachite green. Inorg Chem Commun 172:113669. https://doi.org/10.1016/j.inoche.2024.113669
75. Su D, Xu W, Yang D, Lei J, Liu J, Chen C, O'Hare D (2025) In Situ Growth of ZnAl-LDH on Biomass Carbon for Highly Efficient Photodegradation of Malachite Green (MG) From Water. Appl Org Chem 39(1):e7942. https://doi.org/10.1002/aoc.7942
76. Zhang P, O'Connor D, Wang Y, Jiang L, Xia T, Wang L, Tsang DCW, Ok YS, Hou D (2020) A green biochar/iron oxide composite for methylene blue removal. J Hazard Mater 84:121286. https://doi.org/10.1016/j.jhazmat.2019.121286
77. Lincold MN, Jules ML, Guy NP, Suzanne M, Jacques MB, Sylvain T, Shikuku VO, Tchieta GP (2024) Enhanced adsorption of malachite green onto a composite material activated carbon and iron(III) oxide nanoparticles: isotherm, kinetic, and thermodynamic study. Biomass Conv Bioref 1–20. https://doi.org/10.1007/s13399-024-06277-8
78. Algethami JS, Alhamami MAM, Alqadami AA, Melhi S, Seliem AF (2024) Magnetic hydrochar graftedchitosan for enhanced efficient adsorption of malachite green dye from aqueous solutions: Modeling, adsorption behavior, and mechanism analysis. Int J Biol Macromol 254:127767. https://doi.org/10.1016/j.ijbiomac.2023.127767

Publisher's Note Springer Nature remains neutral with regard to jurisdictional claims in published maps and institutional affiliations.